Title

Charge Instability in Single-Layer TiTe2 Mediated by van der Waals Bonding to Substrates

Journal

Physical Review Letters, 125(17)

ISSN

0031-9007

Authors

Lin, Meng-Kai

Hlevyack, Joseph A

Chen, Peng

et al.

Publication Date

2020-10-23

DOI

10.1103/physrevlett.125.176405

Peer reviewed

Charge Instability in Single-Layer $TiTe_2$ Mediated by van-der-Waals Bonding to Substrates

Meng-Kai Lin[1,2], Joseph A. Hlevyack[1,2], Peng Chen[3], Ro-Ya Liu[1,2,4,5], Sung-Kwan Mo[4], and T.-C. Chiang[1,2,*]

[1]*Department of Physics, University of Illinois at Urbana-Champaign, Urbana, Illinois 61801, USA*

[2]*Frederick Seitz Materials Research Laboratory, University of Illinois at Urbana-Champaign, Urbana, Illinois 61801, USA*

[3]*Key Laboratory of Artificial Structures and Quantum Control (Ministry of Education), Shenyang National Laboratory for Materials Science, and Shanghai Center for Complex Physics, School of Physics and Astronomy, Shanghai Jiao Tong University, Shanghai 200240, China*

[4]*Advanced Light Source, Lawrence Berkeley National Laboratory, Berkeley, California 94720, USA*

[5]*Institute of Physics, Academia Sinica, Taipei 10617, Taiwan*

Corresponding Author

T.-C. Chiang, Email: tcchiang@illinois.edu

Abstract

Single layers of materials, including numerous quasi-two-dimensional transition metal dichalcogenides, are of interest for emergent properties under extreme quantum confinement in reduced dimensions. A key issue, difficult to address and often neglected, is the influence of a substrate on the single-layer properties. We show that even weak van-der-Waals bonding between a single layer and its substrate can yield strong effects. The test system, single-layer $TiTe_2$, shows a (2x2) charge density wave (CDW) below a critical temperature of T_C = 92 K if it is grown on a bilayer graphene. When the same single layer is instead grown on $PtTe_2$ films, its CDW T_C becomes suppressed and varies strongly with the $PtTe_2$ film thickness. This change in substrate $PtTe_2$ thickness does not affect the interfacial epitaxial relationship, but the substrate transforms from a semiconductor with a sizable gap to a semimetal. The experimentally observed trend demonstrates the importance of interfacial electronic interaction. A general implication is that substrate effects are an integral part of single-layer physics.

Introduction

Research on single layers has demonstrated abundant cases of novel properties including lattice and charge distortions, magnetic ordering, Lifshitz or topological electronic transitions, superconductivity, etc. that are drastically different from the corresponding bulk cases[1-18]. Transition metal dichalcogenides (TMDCs)[1-11,16,19-23], which form a huge group of van-der-Waals layered systems, are excellent parent materials for single layers. Many TMDCs exhibit charge density waves (CDWs) involving coupled charge and lattice distortions, which compete against other types of ordering. A few examples of TMDCs that exhibit CDWs include a (2x2x2) phase in bulk $TiSe_2$ below 205 K and a (2x2) phase below 232 K in the single layer[2-4], a (3x3x1) phase in bulk $NbSe_2$ below 33 K and a CDW transition at possibly up to 145 K in the single layer[8,9,19-21],

and a (4x4x3) CDW phase in bulk VSe_2 below 110 K and a $\left(\sqrt{7}\times\sqrt{3}\right)$ phase below 220 K in the single layer[5-7,22,23]. The system of interest for the present study, $TiTe_2$, is an extraordinary case. When grown on a bilayer-graphene-terminated SiC surface (BLG, for short), a single layer of $TiTe_2$ shows a (2x2) CDW transition below T_C = 92 K, but thicker films even at just two layers do not show any CDW transitions[1]. The single layer, with its singular behavior, is evidently highly sensitive to what lies underneath it, which makes it a particularly sensitive test case for investigating substrate coupling effects. A basic understanding of the coupling phenomenon is important for engineering single layers for applications.

We employ *N*-layer films of $PtTe_2$ as the substrate for single-layer $TiTe_2$, where N = 0, 1, … 4, for a systematic investigation of the substrate coupling effects. At N = 0, the substrate reduces to a BLG. This is one of the most weakly interacting substrates. A small lattice constant of BLG means that the surface is densely packed with a small surface corrugation potential. Single-layer $TiTe_2$ atop assumes an unstrained parallel epitaxy structure[1]; the lattice incommensuration averages out any interfacial directional bonding. Furthermore, BLG has a very large band gap near the zone center. The π bands cross the Fermi level far away from the zone center and have a very low density of states near the Fermi level. All of these factors combined make the single-layer film of $TiTe_2$ on top of the BLG nearly freestanding. $TiTe_2$ grown on *N*-layer $PtTe_2$ also assumes an incommensurate parallel epitaxy structure although with a smaller lattice mismatch. At N = 1, $PtTe_2$ is a semiconductor with a sizable gap[11]. The lack of electronic states near the Fermi level suggests a weak interfacial electronic interaction with the overlayer. At N = 2 and above, $PtTe_2$ turns into a semimetal with an increasing number of bands crossing the Fermi level. The incommensurate interfacial bonding remains of the van-del-Waals type despite the increasing metallicity of the substrate. The central question is, how the CDW transition in the $TiTe_2$ single

layer might be affected by the changes in the substrate electronic structure as *N* increases. Our systematic study based on angle-resolved photoemission spectroscopy (ARPES) and theory shows that resonant coupling near the Fermi level accompanied by the metallicity changes suppresses the CDW in the single-layer $TiTe_2$.

Results

ARPES maps and CDW of single-layer $TiTe_2$ on BLG.

As the base results for comparison, Fig. 1a and b show ARPES maps of single-layer $TiTe_2$ on BLG along the $\overline{\Gamma M}$ direction for the (1x1) normal phase at 300 K and the (2x2) CDW phase at 25 K, respectively. No ARPES features from the BLG are present in the data, as they appear elsewhere in the energy-momentum space. The results, in agreement with prior studies[1], show three metallic bands crossing the Fermi level at 300 K: two concave Te 5*p* valence bands centered about the zone center $\overline{\Gamma}$ and a convex Ti 3*d* conduction band centered about the $\overline{M}$ point at the zone boundary. The ARPES map at 25 K appears sharper because of reduced thermal broadening. Additionally, weak replicas of the valence bands now appear centered about $\overline{M}$, which arise from (2x2) folding in the CDW phase. The folded band features are faint in the original data but become readily seen by comparing the zoomed-in second-derivative maps around the conduction band minimum in Fig. 1c and d for the sample at 300 and 25 K, respectively.

ARPES maps and CDW of single-layer $TiTe_2$ on single-layer $PtTe_2$.

Similar ARPES results were taken from a single layer of $TiTe_2$ grown on a single layer of $PtTe_2$, which was itself grown on a BLG. Fig. 2a and b show ARPES maps at 300 and 25 K, respectively, for the single-layer $PtTe_2$ before $TiTe_2$ growth. The corresponding second-derivative maps are shown in Fig. 2c and d together with the theoretical band dispersion relations (dashed

curves)[11]. The data for the two temperatures are similar, but the bands at 25 K are sharper because of reduced thermal broadening. The ARPES results confirm that single-layer $PtTe_2$ is a semiconductor; the gap is 0.79 eV from theory[11]. Fig. 2e and f show ARPES results after the addition of a $TiTe_2$ single layer on top. The results, dominated by the $TiTe_2$ emission features, are very similar to those seen in Fig. 1. Zoomed-in second-derivative ARPES maps around the conduction band minimum at $\bar{M}$ taken at 300 and 25 K are presented in Fig. 2g and h, respectively. The 25 K data show folded valence bands, similar to those seen in Fig. 1d, indicating that single-layer $TiTe_2$ on single-layer $PtTe_2$ also exhibits a CDW at 25 K.

Substrate thickness-dependent band structure and CDW transition.

ARPES maps taken from single-layer $TiTe_2$ grown on N-layer $PtTe_2$ films, with N = 0, 1, … 4, on BLG are shown in Fig. 3a and b for sample temperature at 300 and 25 K, respectively. Fig 3a also contains calculated band dispersion relations for freestanding single-layer $TiTe_2$ for comparison[1]. Shown in the Supplementary Information are the corresponding ARPES maps for the N-layer $PtTe_2$ films before $TiTe_2$ growth[24], from which it is evident that $PtTe_2$ becomes a semimetal already at N = 2, and the system remains semimetallic with more bands crossing the Fermi level as N increases. Second-derivative ARPES maps taken at 25 K near the conduction band minimum at $\bar{M}$ of $TiTe_2$ for the bare BLG substrate and for single-layer $TiTe_2$ on N = 0, 1, … 4 layers of $PtTe_2$ are presented in Fig. 3c. Valence band folding caused by CDW formation is evident for N = 0 and 1, but not for larger N, and the folded-band features at N = 1 are weaker than those for N = 0. Thus, the CDW state at 25 K is the strongest for N = 0, weaker for N = 1, and fully suppressed at higher N. The measured ARPES intensity of the folded bands is a measure of the CDW order parameter. The red squares in Fig. 3d represent integrated ARPES intensities in the yellow box indicated in Fig. 3c for N = 0 as a function of temperature, and the curve is a fit

based on the BCS mean-field equation[2-4], from which a transition temperature of T_C = 95 ± 3 K is extracted. A similar analysis for N = 1 (blue circles in Fig. 3d) yields a lower CDW T_C = 65 ± 3 K. No CDW transitions are seen for N = 2, 3, and 4. Evidently, the CDW in $TiTe_2$ is weakened and eventually suppressed by increasing the thickness of the $PtTe_2$ substrate film.

CDW suppression by electronic coupling to the substrate.

The trend of CDW suppression as a function of N can be correlated with the evolution of the $PtTe_2$ film's electronic structure. The band structure around the Fermi level for single-layer $TiTe_2$, shown as blue curves in Fig. 4a-e, is superimposed on the band structures of the different substrates[1,11]. If the $TiTe_2$ overlayer and substrate valence band structures closely match in energy-momentum space near the Fermi level, resonant coupling of the electronic states across the interface can arise and make the overlayer less freestanding-like, thus affecting the overlayer properties. Visual inspection reveals that, within 0.5 eV of the Fermi level (indicated by the shaded bands in Fig. 4a-e), there is a huge mismatch for N = 0, a somewhat better match for N = 1, and a good match for N = 2 and above.

To quantify the analysis, we define a band-match function χ as an integral from E_B = -0.5 eV to the Fermi level at E = 0 in terms of the momentum mismatch between the $TiTe_2$ overlayer bands, indexed by i, and the N-layer substrate bands, indexed by j:

$$\chi(N) = \int_{E_B}^{0} dE \sum_{i}^{\text{Overlayer}} \left\langle \frac{1}{\left| k_i(E) - k_j^N(E) + i\Gamma \right|^2} \right\rangle_j \qquad (1)$$

where the average is taken over the substrate bands, and Γ is the combined momentum broadening of the bands, which can be deduced from the measured ARPES band widths. The evaluation of χ is summed over $\overline{\Gamma K}$ and $\overline{\Gamma M}$. A large χ means a good band match, and vice versa. Fig. 4f shows

the computed χ function for N = 0, 1, … 4. For simplicity, we have used an average value of Γ = 0.2 Å^{-1} in the evaluation, but the shape of the χ function remains essentially the same for Γ ranging from 0.05 to 0.3 Å^{-1}. Likewise, the shape of χ is insensitive to the choice of E_B within the range of -0.3 to -0.8 eV. This insensitivity is demonstrated in the Supplementary Information[24]. As seen in Fig. 4f, the band-match function rises rapidly from N = 0 to 1 and to 2 and saturates afterwards. This correlates well with the observed trend for the CDW transition: T_C = 95 and 65 K for N = 0 and 1, respectively, and no CDW is observed for N = 2, 3, and 4. A good band match leads to CDW suppression.

Discussion and implications.

Our observation strongly suggests that the (2x2) CDW in single-layer $TiTe_2$ is a two-dimensional property, and electronic coupling to the substrate weakens it. With increasing N, the interfacial bonding remains of the van-der-Waals type. However, the metallicity of the substrate changes, and the electronic coupling as measured by the band-match function increases. At N = 2 and beyond, the (2x2) CDW phase becomes suppressed. The increased overlayer-substrate coupling is also evident from the evolution of the ARPES maps seen in Fig. 3c, where the conduction band minimum shifts slightly down in energy and the bandwidth broadens for increasing N. The changes are most notable between N = 1 and 2, which correlates well with the suppression of the CDW. Similar band renormalization and bandwidth changes are seen for the other bands in Fig. 3a and b, which suggest increased electronic coupling to the substrate and the development of three dimensionality in the system. Conceptually, the best electronic band match occurs when the single-layer $TiTe_2$ is placed on top of another single layer of $TiTe_2$. The resulting bilayer of $TiTe_2$ shows no CDW[1], which is consistent with the trend discussed above. The premise of CDW modification by overlayer-substrate coupling should be broadly applicable to other van-

der-Waals heterostructures. As a further demonstration, an ARPES study of single-layer $TiTe_2$ grown on a small-gap semiconductor, single-layer $TiSe_2$, is presented in the Supplementary Information[24]; no CDW is observed in this system down to 25 K because of a good band match between single layers of $TiTe_2$ and $TiSe_2$.

Our systematic investigation of the CDW in single-layer $TiTe_2$ upon tuning the substrate electronic structure leads us to conclude that even incommensurate van-der-Waals bonding, which is expected to be very weak, can lead to nontrivial modifications of the single-layer properties. Single layers are of great interest for their potential novel properties caused by extreme quantum confinement and reduced dimensionality, but the vast majority of studies of single layers to date generally sidestep the issue of substrate interaction. Our results provide important physical insights into the coupling issue and demonstrate the potential for tuning single-layer properties by substrate engineering.

Methods

Substrates of 6H-SiC(0001) were annealed repeatedly to form a well-ordered BLG-terminated surface on the Si-terminated side. $PtTe_2$ films were grown at a rate of one layer per 50 minutes by co-deposition of Pt and Te from an electron-beam evaporator and an effusion cell, respectively, under a high Te overpressure with the substrate maintained at 280 $^{\circ}$C[11]. Afterwards, a single layer of $TiTe_2$ was grown on top of the $PtTe_2$ films in a similar manner[1,11]. Characterization of the film growth processes and measurements of the band structure by ARPES were performed using a Scienta R4000 analyzer and a Scienta Omicron VUV5K helium lamp operating at 21.22 eV as the light source. The preparation of single-layer $TiTe_2$ on $TiSe_2$ was done similarly; ARPES

measurements of this system were performed using 58-eV photons at beamline 10.0.1.1, Advanced Light Source.

Acknowledgements

This work is supported by the U.S. Department of Energy (DOE), Office of Science (OS), Office of Basic Energy Sciences, Division of Materials Science and Engineering, under Grant No. DE-FG02-07ER46383 (T.C.C.). This research used resources of the Advanced Light Source, which is a DOE Office of Science User Facility under contract No. DE-AC02-05CH11231.

Author Contributions

M.K.L. and T.C.C. designed the experiment. M.K.L. and J.A.H. performed MBE film growth. M.K.L., with the aid of J.A.H., P.C., R.Y.L., S.K.M, and T.C.C., performed the ARPES measurements and data analysis. M.K.L. and T.C.C. interpreted the data and wrote the paper. All authors participated in discussions and revisions of the manuscript.

Competing interests

The authors declare no competing interests.

References

1. Chen, P., et al. Emergence of Charge Density Waves and a Pseudogap in Single-Layer $TiTe_2$. *Nat. Commun.* **8**, 516 (2017).

2. Chen, P., et al. Charge Density Wave Transition in Single-Layer Titanium Diselenide. *Nat. Commun.* **6**, 8943 (2015).

3. Fang, X. Y., Hong, H., Chen, P., Chiang, T.-C. X-Ray Study of the Charge-Density-Wave Transition in Single-Layer $TiSe_2$. *Phys. Rev. B* **95**, 201409 (2017).

4. Chen, P., et al. Dimensional Effects on the Charge Density Waves in Ultrathin Films of $TiSe_2$. *Nano Lett.* **16**, 6331 (2016).

5. Chen, P., et al. Unique Gap Structure and Symmetry of the Charge Density Wave in Single-Layer VSe_2. *Phys. Rev. Lett.* **121**, 196402 (2018).

6. Feng, J., et al. Electronic Structure and Enhanced Charge-Density Wave Order of Monolayer VSe_2. *Nano Lett.* **18**, 4493 (2018).

7. Duvjir, G., et al. Emergence of a Metal-Insulator Transition and High-Temperature Charge-Density Waves in VSe_2 at the Monolayer Limit. *Nano Lett.* **18**, 5432 (2018).

8. Ugeda, M. M., et al. Characterization of Collective Ground States in Single-Layer $NbSe_2$. *Nat. Phys.* **12**, 92 (2016).

9. Xi, X., et al. Strongly Enhanced Charge-Density-Wave Order in Monolayer $NbSe_2$. *Nat. Nanotechnol.* **10**, 765 (2015).

10. Guster, B. Robles, R., Pruneda, M., Canadell, E., Ordejón, P. 2x2 Charge Density Wave in Single-Layer $TiTe_2$. *2D Mater.* **6**, 015027 (2019).

11. Lin, M. K. et al. Dimensionality-Mediated Semimetal-Semiconductor Transition in Ultrathin $PtTe_2$ Films. *Phys. Rev. Lett.* **124**, 036402 (2020).

12. Bian, G. et al. Engineering Electronic Structure of a Two-Dimensional Topological Insulator Bi(111) Bilayer on Sb Nanofilms by Quantum Confinement Effect. *ACS Nano* **10**, 3859 (2016).

13. Zhang, P., Liu, Z., Duan, W., Liu, F., and Wu, J. Topological and Electronic Transitions in a Sb(111) nanofilm: The Interplay Between Quantum Confinement and Surface Effect. *Phys. Rev. B* **85**, 201410 (2012).

14. Liu, Y., et al. Thickness-Dependent Magnetic Order in CrI_3 single crystals. *Sci. Rep.* **9**, 13599 (2019).

15. Huang, B., et al. Layer-Dependent Ferromagnetism in a van der Waals Crystal Down to the Monolayer Limit. *Nature* **546**, 8 (2017).

16. Wang, H., et al. High-Quality Monolayer Superconductor $NbSe_2$ Grown by Chemical Vapour Deposition. *Nat. Commun.* **8**, 394 (2017).

17. Ge, J. F., et al. Superconductivity Above 100 K in Single-Layer FeSe Films on Doped $SrTiO_3$. *Nat. Mater.* **14**, 285 (2015).

18. Tan, S., et al. Interface-Induced Superconductivity and Strain-Dependent Spin Density Waves in $FeSe_2/SrTiO_3$ Thin Films. *Nat. Mater.* **12**, 634 (2013).

19. Arguello, C. J., et al. Visualizing the Charge Density Wave Transition in 2*H*-$NbSe_2$ in Real Space. *Phys. Rev. B* **89**, 235115 (2014).

20. Wilson, J. A., Di Salvo, F. J., and Mahajan, S., Charge-Density Waves and Superlattices in the Metallic Layered Transition Metal Dichalcogenides. *Adv. Phys.* **50**, 1171 (2001).

21. Moncton, D. E., Axe, J. D., and DiSalvo, F. J. Study of Superlattice Formation in 2*H*-$NbSe_2$ and 2*H*-$TaSe_2$ by Neutron Scattering. *Phys. Rev. Lett.* **34**, 734 (1975).

22. Tsutsumi, K. X-Ray-Diffraction of the Periodic Lattice Distortion Associated with a Charge-Density Wave in 1*T*-VSe_2. *Phys. Rev. B* **26**, 5756 (1982).

23. Eaglesham, D. J., Withers, R. L., and Bird, D. M., Charge-Density-Wave Transitions in 1T-VSe_2. *J. Phys. C: Solid State phys.* **19**, 359 (1986).

24. Supplementary Information.

Figure 1 ARPES from single-layer $TiTe_2$ on BLG. a, b ARPES maps along the $\overline{\Gamma M}$ direction taken at 300 and 25 K, respectively, using 21.22 eV photons. **c, d** Zoomed-in second-derivative ARPES maps near the conduction band minimum around $\bar{M}$ taken at 300 and 25 K, respectively.

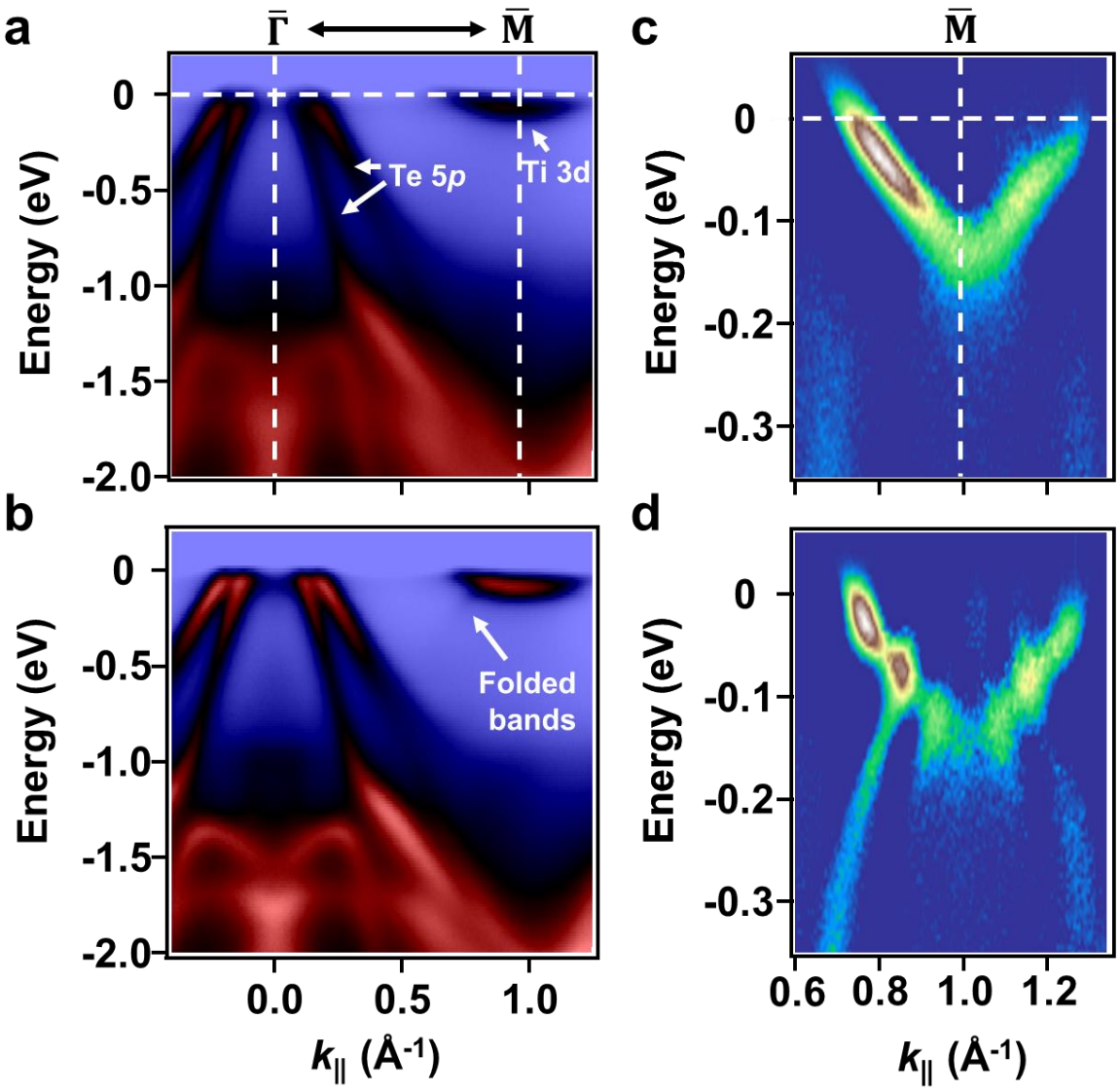

Figure 2 ARPES from single-layer $PtTe_2$ and single-layer $TiTe_2$ on single-layer $PtTe_2$. a, b ARPES maps of single-layer $PtTe_2$ along $\overline{\Gamma M}$ taken at 300 and 25 K, respectively, using 21.22 eV photons. **c, d** Corresponding second-derivative maps with superimposed theoretical band structure. **e, f** ARPES maps of single-layer $TiTe_2$ on single-layer $PtTe_2$ along $\overline{\Gamma M}$ taken at 300 and 25 K, respectively. **g, h** Corresponding zoomed-in second-derivate maps near the conduction band minimum at $\overline{M}$.

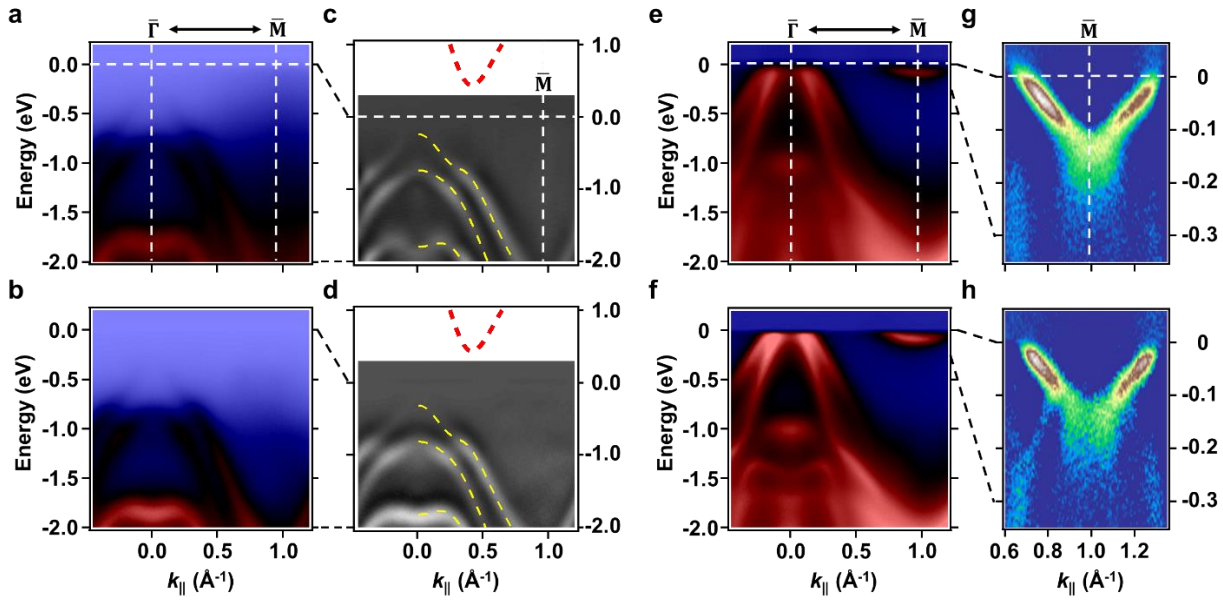

Figure 3 ARPES maps for single-layer $TiTe_2$ on *N*-layer $PtTe_2$. a, b ARPES maps along $\overline{\Gamma M}$ for N = 0, 1, … 4 taken at 300 and 25 K, respectively. The band structure of single-layer $TiTe_2$ (dashed curves) is included in **a** for comparison. **c** Second-derivative maps near the conduction band minimum at 25 K for bare BLG and the $TiTe_2/PtTe_2$ samples for N = 0, 1, … 4. **d** ARPES intensity of the folded band (integrated over a box as indicated in **c** for N = 0) as a function of temperature for the different N's. The curves are BCS mean-field fits.

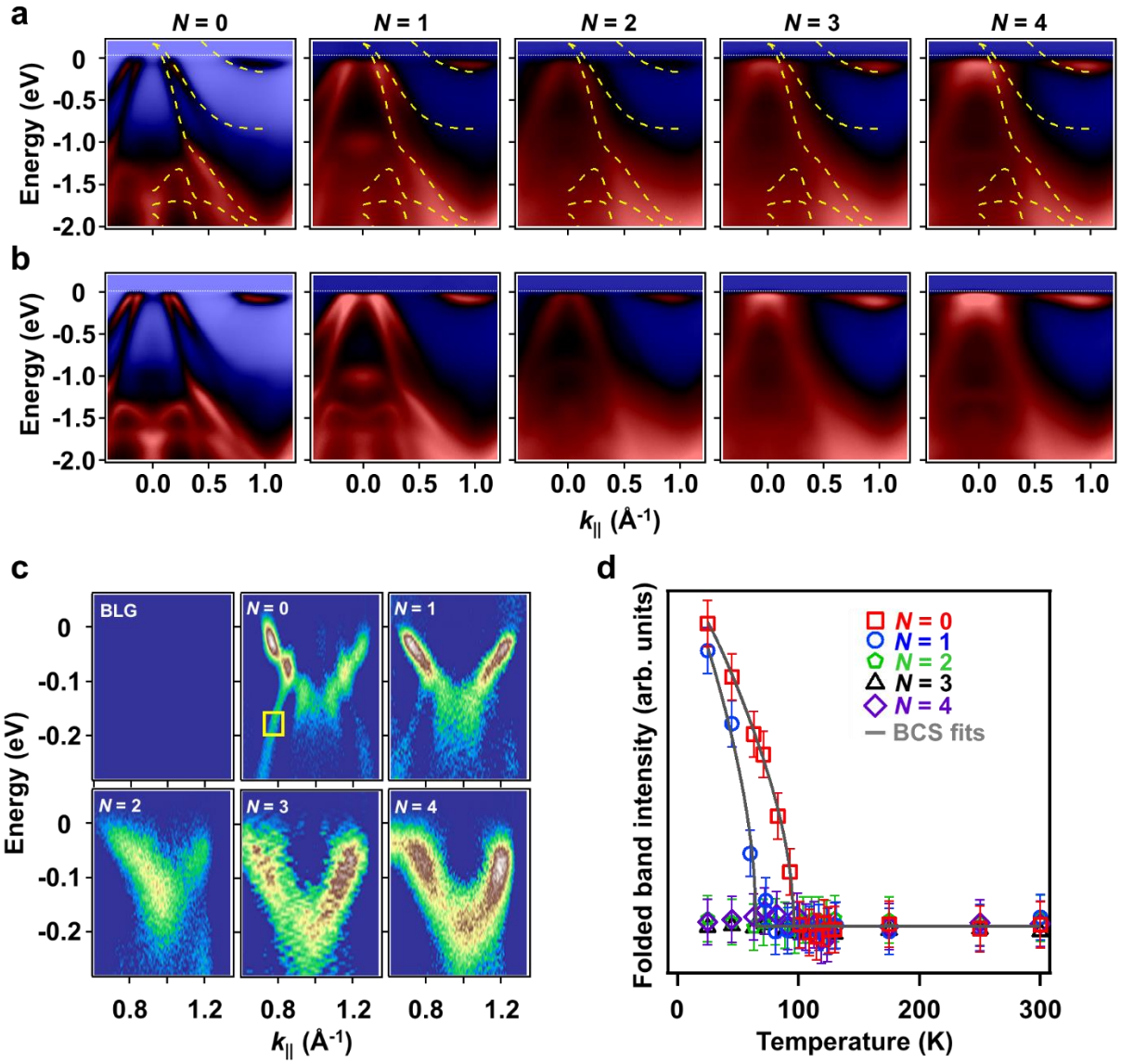

Figure 4 Electronic structure and band-match function χ. a-e Theoretical band structures for single-layer $TiTe_2$ (blue curves) and the $PtTe_2$/BLG substrate for N = 0, 1, … 4, respectively, along the $\bar{K} - \bar{\Gamma} - \bar{M}$ directions. The Brillouin zone boundaries for BLG, $TiTe_2$, and $PtTe_2$ are indicated. The horizontal shaded band in **a**-**e** indicates the energy range used to evaluate χ. **f** The band-match function χ as a function of N. The color shading indicates weakening of the CDW state from N = 0 to 1 and suppression of the CDW state at N = 2 and beyond.